Origin of the Nonlinear Optical Response in Organotetrel Molecules, (Hetero)adamantane-Type Clusters with Organic Substituents, and Related Species

Ferdinand Ziese,* Jie Wang,* Irán Rojas León,* Stefanie Dehnen,* and Simone Sanna*

ABSTRACT: The nonlinear optical response of (hetero)adamantane-type clusters and organotetrel molecules with the general formula $[(RT)_4E_6]$ and $[TR_4]$ (T = group 14, R = organic substituents, E = S, CH_2) is investigated from first p rinciples. T hese c lusters h ave been reported to efficiently co nvert in frared ra diation in to wh ite li ght and are therefore extremely attractive functional materials for a multitude of applications. We demonstrate that the optical nonlinearities of the clusters in the range from 0 to 3 eV have their origin in electronic transitions within the substituents. The cluster core does not directly take part to the generation process; however, it strongly affects the intensity of the linear and nonlinear response. The relationships between optical properties and cluster symmetry, stoichiometry, substituent field, core composition, and further structural characteristics are investigated by systematical variation of R and T. This also demonstrates the possibility to finely tune the intensity as well as the frequency dependence of the optical response. Upon formation of cluster dimers, the intensity of the nonlinearities depends on the overall dimer geometry. In the case of heterogeneous dimers, the optical response strongly resembles that of a dominant cluster. Similarly, upon formation of cluster crystals, the compound inherits the optical characteristics of the parent molecules.

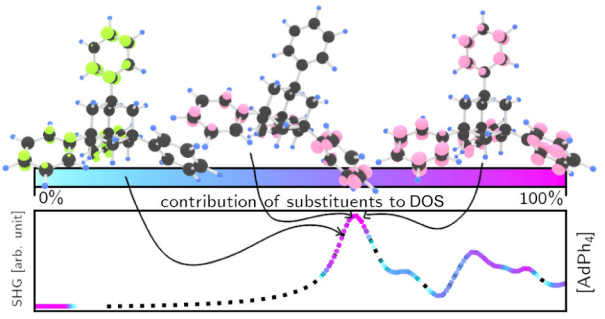

INTRODUCTION

Molecular materials with nonlinear optical properties[1−5] are currently in the focus of the scientific community due to potential applications in a multitude of technologies, including illumination and further devices in everyday's life. In particular, a novel class of molecular compounds exhibiting extreme nonlinear optical properties that allow to convert infrared (IR) light from a continuous wave laser diode into a broad white-light emission (WLE)[6−8] has been intensively investigated in the last years. The WLE, more correctly referred to as a supercontinuum generation, denominates the conversion of monochromatic light into an extremely wide spectrum by a nonlinear medium.[9−11] The resulting spectrum may be broad enough to embrace the whole visible spectral range, finally resulting in white light emission.

While traditional white light sources based on inorganic phosphors or inorganic and organic semiconductors[12−14] require very expensive pulsed laser sources, generation of white light by means of IR lasers is 4 orders of magnitude cheaper, and thus represents a pathway to a sustainable and ecologically as well as economically friendly technology.[15−17] In particular, the possibility to process the compounds, which typically exist as powders, in form of glasses, might represent the key to a broad application.[18] Unfortunately, the physical mechanisms underlying supercontinuum generation are far from being understood. It is indeed known as a combination of many nonlinear optical effects, such as self-phase and cross-phase modulation, four-wave mixing, or solitonic phenomena.[19−22] The single processes can also contribute to different extents for different compounds. In order to gain insight into the origin of the nonlinear optical response of the mentioned molecular compounds, we investigate from first-principles inorganic adamantane-type compounds and organic adamantane derivatives that share the general formula $[(RT)_4E_6]$. Thereby, R is an organic substituent, T is a group 14 atom (C, Si, Ge, and Sn), and E is an S or CH_2. These compounds bear a high potential as white light emitters, and it has even be suggested that they can replace established sources.[18] For this reason, the past few years have witnessed rapid progress of related research. Thus, although only 10 years ago almost nothing was known concerning the optical response of these molecular compounds, recent studies revealed several interesting aspects. As a general rule of thumb, a high degree of structural disorder as well as

aromatic molecules as substituents R are considered prerequisites for the WLE.[23,24] All the clusters showing WLE investigated so far are characterized by strong optical nonlinearities of second and third order, at least as strong as that of widespread optically nonlinear functional materials such as crystalline ferroelectrics.[25−29] Theoretical models have shown that the optical response of the molecular crystals is generally very similar to that of the parent molecules[18,30,31] and can be interpreted in terms of multiphoton processes. The optical nonlinearities are moreover enhanced by disorder and structural asymmetry, in particular by heterogeneous core composition.[18]

The optical nonlinearities feature high peaks and low deeps at which the optical coefficients are almost quenched. The optical response is thus strongly dependent on the incident photon energy relative to the HOMO−LUMO gap. Interestingly, WLE is achieved by an excitation in a generally nonresonant region of the nonlinear optical spectrum (1.1−1.3 eV), however, where the onset of the optical nonlinearities is already pronounced.[25] As this spectral region is followed by a steep gradient of the nonlinear optical susceptibilities, the WLE efficiency might be further increased, provided that it correlates (as currently assumed) with the optical nonlinearities.

The investigated structures can be viewed as modified adamantane core molecules or substructures of these. Recently, we also investigated the optical response of mixed dimer structures in addition to homogeneous dimers. *Fused* cores resulting in interesting symmetry effects are also part of our path toward understanding the possibilities to tune the nonlinear optical properties.[1]

In the present work, we explore by means of atomistic calculations how single factors (structural and electronic degrees of freedom, chemical composition, etc.) as well as their intertwinement determine the nonlinear optical response of the adamantane-shaped $[(RT)_4E_6]$ clusters. The spectroscopic signatures of a multitude of investigated systems are predicted. The correlation between structural/electronic features and optical response furthermore leads to the identification of the prerequisites for the optical nonlinearities, thus inspiring the synthetization of new compounds with tailored optical properties.

METHODOLOGY

The classes of molecular systems investigated in this work are listed in Figure 1. Figure 1a depicts a tetraphenyl adamantane cluster, color coded in Figure 1a′ to distinguish what we consider to be the core and the substituents. Figure 1b shows a single-atom core structure with one substituent. This can also be interpreted as a substituent substructure, as shown in Figure 1b′. Considering the H atoms connected to the core as substituents or part of the core is arbitrary. However, as we show in the following, this choice does not impact the optical response of the (sub)structure significantly. The same color coding is used to show an example of a *fused* core in Figure 3c,c′. In general, all structures we investigated are saturated by H atoms if dangling bonds are present.

The calculation of the nonlinear optical response of the molecular systems described above can be understood as a two-step process. The first step is a structural optimization, which we perform within density functional theory (DFT) using the Vienna Ab initio Software Package (VASP).[32−34] The Perdew−Burke−Ernzerhof (PBE) functional[35] in combination with projector augmented wave (PAW) potentials are employed.[36,37] Dispersion forces are accounted for by means of the vdW DFT-D3 method with Becke−Johnson damping function.[38,39] The molecules in the gas phase were all modeled within a box sized so that the molecule can be considered isolated, resulting in boxes with edges of ≈33 to 37 Å. The force threshold is in all cases ≤0.005 eV/Å. The atomic coordinates of the optimized structures can be found in the Supporting Information.

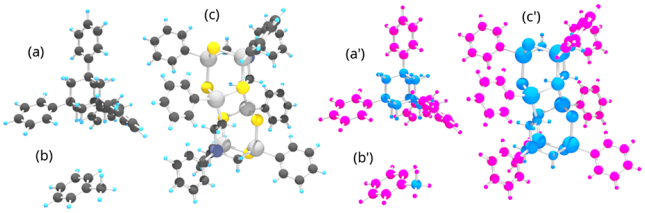

Figure 1. (a) $[AdPh_4]$ adamantane-core molecule with phenyl substituents, (b) simplified model $[CPhH_3]$ molecule with a single atom core, (c) $[(PhSi)(CH_2)_4(PhSn)_3S_3]_2$ dimer structure with a so-called *fused* core. The three structures on the left are color coded by species: H, light blue; C, black; Sn, light gray; Si, dark blue-gray; and S, yellow. For the three structures (a′,b′,c′) on the right, the colors do not identify the atomic species, but the molecular substructures and their categorization discussed above. The core is depicted in turquoise, and the substituents are in purple.

For the final step, we need a precursor calculation, which outputs the wave functions used for the actual optics calculation. We calculate the electronic ground state using the Quantum Espresso package.[40,41] The (semi)local PBE functional is used for Quantum Espresso calculations as well;[35] however, SG15[42] ONCV potentials were used[43,44] instead of PAWs. The electronic ground state calculated using Quantum Espresso and the ONCV potentials fit well to the comparable calculations conducted using VASP and PAWs. Within the adopted approach, we chose the computational parameters in order to ensure numerical convergence of the electronic structures.

In the final step, we perform calculations within the real time approach[45] to compute the nonlinear optics of the investigated compounds. In particular, hyperpolarizabilities of virtually any order (in our case, $\chi^{(2)}$) are calculated by developing the dynamical polarization in a power series of the applied monochromatic laser field. The dynamical polarization is calculated within the Berry-phase formulation.[46] The second order optical response of the molecules in the gas phase is given by the spatial average of the absolute value of the $\chi^{(2)}_{SHG}$ tensor. The calculations are performed within the IPA using the YAMBO[47] code. The numerical parameters, such as propagation time, time-step size, and spectral broadening, are chosen to ensure convergence of the nonlinear optical spectra. The numerical values are given in the Supporting Information.

We remark that an approach beyond the IPA, including many-body effects and electron−hole attraction, is needed, in principle, to obtain numerically accurate optical spectra. However, such an approach is computationally expensive and not suitable for an extended investigation as the one presented in the following. Yet, the calculations within the IPA presented in the following represent a first estimate of the nonlinear optical response and, more importantly, allow for a comparison of the relative magnitude of the optical nonlinearities of different molecules.

At finite temperatures, each atom or atomic group in the molecule vibrates or rotates about their average position. This motion modifies the topology of the molecule by a given (possibly anisotropic) displacement pattern. Depending on the

energy landscape, some parts of the molecule may display particularly large amplitudes of motion. These effects have been shown to contribute to the SHG effect.[48] As we calculate the optical response with static molecular structures representing energy minima, contributions to the nonlinear optical response originating from the atomic motion are neglected.

RESULTS

Origin of the Nonlinear Optical Response. As a first step toward the understanding of the origin of the optical nonlinearites, we correlate the electronic energy levels of the isolated clusters and the electronic transitions involved in the nonlinear optical response. The latter is exemplarily quantified in the following by the second order optical coefficients for frequency doubling (second harmonic generation (SHG) coefficients). Thereby, we discuss exemplarily the prototypical [$AdPh_4$] cluster represented in Figure 1a as a model system. For this system, we consider electronic transitions from occupied orbital groups (named *origin* and labeled by "o″) into empty orbital groups (named *target* and labeled by "t″). The electronic levels are shown in Figure 2 in the left panel. The light/dark gray alternating colors for the occupied orbital groups are selected to distinguish individual orbital groups. The unoccupied orbital groups are colored individually instead. As an approximation, the orbitals are grouped into one *effective* orbital group if they are within an energy interval ΔE = 0.1 eV.[2]

In the right panel of Figure 2, the SHG response is shown as a blue solid line, rotated and scaled by a factor of 2 to share the axis with the electronic energy values.

We now consider electronic transitions from the origin to target states. The origin orbital groups are counted energy downward from the highest occupied one, while the target orbital groups are counted upward from the lowest unoccupied. To simulate the electronic transitions, we calculated the convolution of all origin groups with a single target group individually. The last information contained in Figure 2 is thus the convolution $o*t$, which is plotted in front of the SHG spectrum. The convolution is color coded as the targeted group. The transparency of $o*t$ roughly indicates a *density* of energy values.[3] Figure 2 contains the electronic levels, the calculated SHG spectrum, and a convolution of all occupied orbitals with a single target orbital group.

For interpretation of the SHG spectra, we focus on energies between 0 and 3 eV. This interval covers the technologically relevant energy range for the applications proposed so far. A discussion of higher energy spectral features is, although interesting, beyond the goal of the present manuscript.

In order to identify which electronic transition has the largest contribution to a peak in the SHG spectrum, we correlate the peaks of the convolution $o*t$ with the peaks of the SHG spectrum. To this end, the electronic energy levels and $o*t$ for t = 0, t = 1, t = 2, and t = 3 are shifted downward by the amount corresponding to the distance of the respective target orbital group to the LUMO. This results in larger shifts downward to *reach* higher unoccupied targeted groups.

A large convolution at the same energy as the SHG peaks suggests that the corresponding transition has a large contribution to the SHG intensity. Although this approach does not allow a quantitative analysis of the contribution of the single electronic transitions to the optical nonlinearities, it allows to immediately qualitatively analyze the nonlinear optical response.

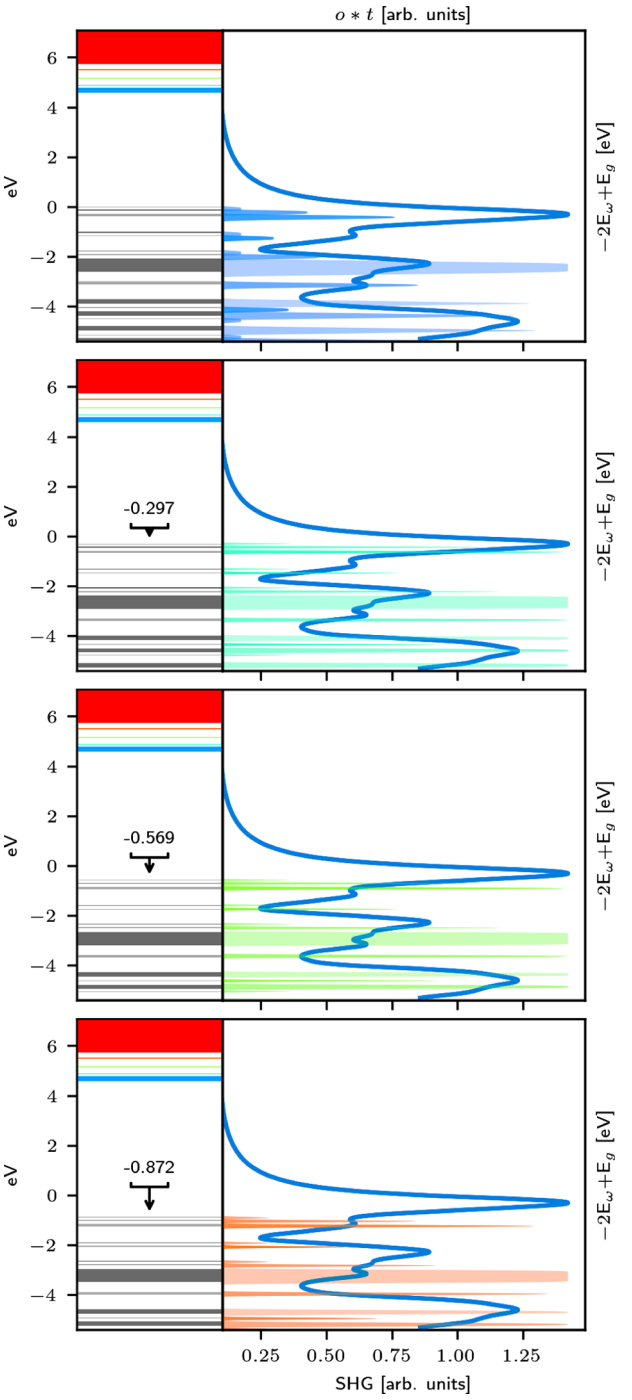

Figure 2. Orbital group energy values of [$AdPh_4$] with the corresponding scaled and shifted SHG response. The energy values of the origin (occupied) orbital groups are shifted for a direct transition to the respective target (unoccupied) orbital group 0, 1, 2, and 3.

Further insight becomes available when the electronic states involved in the transitions with the largest contribution to the SHG signal according to our approach are visualized in real space.

To this end, we calculate the charge densities ρ of the considered orbital groups and the overlap of $\rho_o \cdot \rho_t = \rho_{overlap}$. The latter is shown in Figure 3. In this figure, $\rho_{overlap}$ is plotted for $o, t \in [0, 1, 2]$. Thus, $\rho_{overlap}$ for o = 0 and t = 0 is the spatial overlap of the orbital groups containing HOMO and LUMO, and $\rho_{overlap}$ for o = 0 and t = 1 is the spatial overlap of the orbital

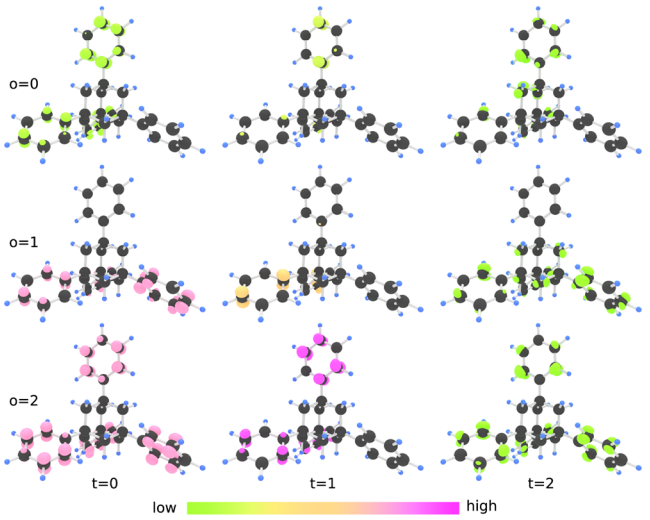

Figure 3. Overlap ρ_{overlap} of *origin* (o) and *target* (t) orbitals, color coded with respect to the overlap magnitude and normalized by the number of orbitals in the respective orbital groups. C atoms are black, and H atoms are light blue.

groups containing HOMO and those containing higher unoccupied orbitals. The displayed values for ρ_{overlap} are normalized by the number of energetic levels in the respective orbital group. This allows us to compare orbital groups with different energy *widths* on the same scale.

For the sake of clarity, we do not show in Figure 3 the isosurfaces with the same numerical value (some would be very extended, other vanishing small). Instead, we color code the magnitude of the overlap and show similarly extended isosurfaces representing ρ_{overlap}.

As we show in the following, transitions between orbital groups with high energy convolution values and with high spatial overlap correlate with the intensity of the optical nonlinearities. These transitions are considered to yield a high contribution to the SHG intensity. This allows us to determine the spatial region of the cluster where the electronic transitions and thus the optical nonlinearities have their origin.

It becomes clear at a first sight at Figure 3 that ρ_{overlap} for o, $t \in [0, 1, 2]$, i.e., for all possible electronic transition in the energy region at which the first SHG peaks occur, is almost completely localized at the phenyl substituents. Moreover, the combinations of *origin* and *target* orbital groups with stronger overlap magnitude ρ_{overlap} (in pink in Figure 3) are those resulting in a higher convolution in correspondence of the SHG peaks in Figure 2. Thus, we find a strong correlation between all peaks in the low energy region of the SHG spectrum and electronic transitions localized at the substituents.

This is shown in more detail for the first SHG peak in Figure 2. Among all possible $o \rightarrow t$ electronic transitions, only combinations of $o = 0, 1, 2$ and $t = 0, 1, 2$ are transition within the considered energy range and can contribute to the SHG peak. The transition between $o = 0$ and $t = 0$ has a minor energy convolution (see the upper panel of Figure 2) and limited overlap (in green in the upper left panel in Figure 3). The following transitions (especially $o = 1, 2$ and $t = 0, 1$) have much larger energy convolution and spatial overlap. Transitions involving $t = 2$ again have a much lower convolution and overlap and contribute less to the first SHG peak.

To achieve a more complete picture, we put these results into the context of the density of states (DOS), as shown in 4. In turn,

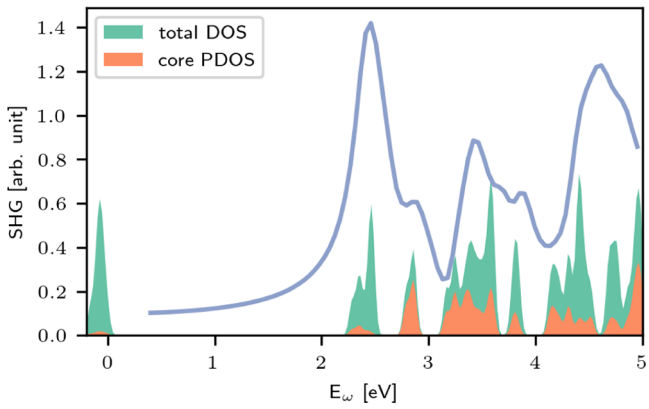

Figure 4. Total and partial DOS (of the core-related states) with a shared energy axis for the SHG spectrum of the $[AdPh_4]$ cluster. The DOS and PDOS are scaled by a factor of 2 to be readily comparable to the SHG spectrum.

the DOS can be compared to the charge density of all *origin* states ρ_o and *target* states ρ_t, which is shown in Figures 5 and 6.[4] First, we observe that the DOS of the $o = 0$ orbital group is almost completely localized at the substituents. This is also shown in real space in Figure 5.

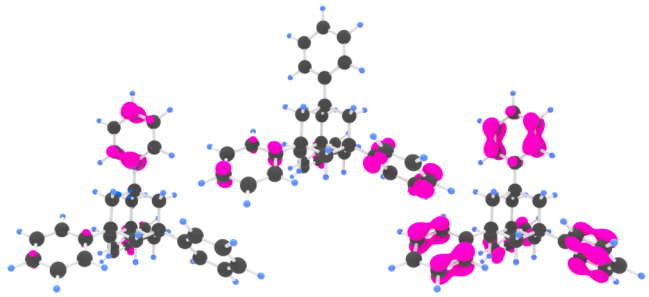

Figure 5. $\rho_o = 0, 1, 2$ from left to right. The coloring of ρ is from blue to pink, defined by the distance from the center of the core and allows a classification into core or substituent localization. A pronounced localization of the substituents is clearly visible. Atomic color as in Figure 3.

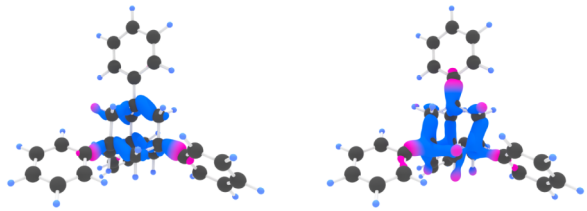

Figure 6. $\rho_o = 3, 4$ from left to right. The coloring of ρ is from blue to pink, defined by the distance from the center of the core and allows a classification into core or substituent localization. A favorable localization in the core is clearly visible. Atomic color as in Figure 3.

The same figure shows that also the orbital groups $o = 1, 2$ are clearly localized on the substituents. For the energetically lower groups $o = 3, 4$, we see in Figure 6 that the core clearly yields the dominating contribution, instead.

A look at the overlaps of $o = 3, 4$ with $t = 0$ in Figure 7 shows that although the orbital groups $o = 3$,4 are mostly localized at the core, their overlap with the target levels $t = 0$ (which energetically would fit to the SHG peak at ≈2.9 eV) is completely localized in the substituent region.

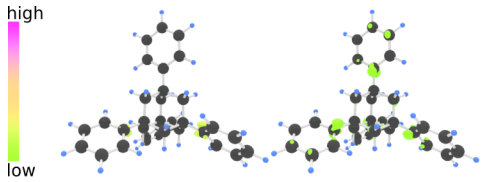

Figure 7. Overlap of o = 3, 4 (left to right) and t = 0 color coded to relative high or low probabilities and normalized for the number of orbitals in the respective orbital groups. A preferable localization on the substituent is visible, although it is clearly shifted to the substituent atoms directly connected to the core structure. Atomic color as in Figure 3.

Figure 8 shows the t = 0, 1, 2 orbital groups from left to right. For t = 0, 1, we can see a dominant substituent localization.

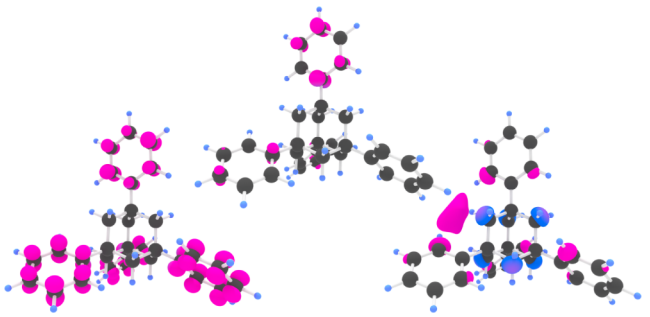

Figure 8. ρ_t = 0, 1, 2 from left to right. The coloring of ρ is from blue to pink, defined by the distance from the center of the core and allows a classification into core or substituent localization. A localization on the substituents is visible for t = 0, 1. For t = 2, the localization is evenly split between the core and substituents. Atomic color as in Figure 3.

Thus, transitions to this group can only result in an overlap localized on the phenyl rings. The first *target* orbital group with some core localization is t = 3. Spatial overlap between *origin* and *target* groups that is at least partially localized at the core is only possible for o, $t \geq 3$. The corresponding electronic transition is outside the energy window of the first SHG peak. For this reason, we conclude that the SHG spectrum below about 3 eV is defined by the substituents. We suggest that the SHG response of [$AdPh_4$] can be attributed to some degree to the adamantane core only above 3 eV, instead. This is well beyond the energy of the HOMO−LUMO transitions.

Having determined that the nonlinear optical response of $AdPh_4$ has its origin in the substituents, it might be possible that *any* tetraphenyl cluster has a similar SHG spectrum below 3 eV. We shall see, indeed, that all tetraphenyl adamantane derivatives share roughly the same nonlinear optical signatures, although their onset depends on the value of the HOMO−LUMO gap. We show indeed in the following that the main characteristics of the SHG response of the tetraphenyl adamantane can be mostly attributed to the characteristics of so-called *substructures*, and therefore, it is not exclusive to clusters containing a complete adamantane core.

To demonstrate this, we show some of the investigated substructures in Figure 9. In Figure 10, we present the SHG response of phenyl adamantane along with those of the substructures.

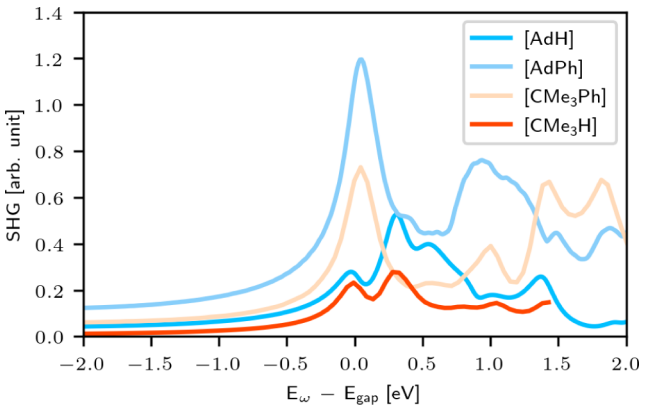

Figure 10. SHG response of an adamantane core, compared to [CMe_3H] and both structures with a phenyl substituent ([AdPh] and [CMe_3Ph]). They are shown with the same color code in Figure 9.

Additionally to adamantane, Figure 10 shows the SHG response of [CMe_3H] which can be considered to be a substructure of an adamantane core. The spectrum of [AdPh] presents the same features as the [$AdPh_4$] SHG spectrum shown in Figure 4, with an obvious redistribution of the spectral weights. The SHG spectra of [AdH] and [CMe_3H] (darker solid lines) are undoubtedly similar. Furthermore, with the addition of a phenyl substituent, both [AdH] and [CMe_3H] exhibit a similar change in their SHG response. This corroborates our suggestion that the low energy region of the SHG spectrum of tetraphenyl adamantane inherits the signatures that can be found in the substructures containing phenyl substituents.

Figure 11 provides the (energy scaled) DOS of [AdPh] and [CMe_3Ph], which is compared with the SHG spectra. The partial DOS of the respective core atoms is represented lighter

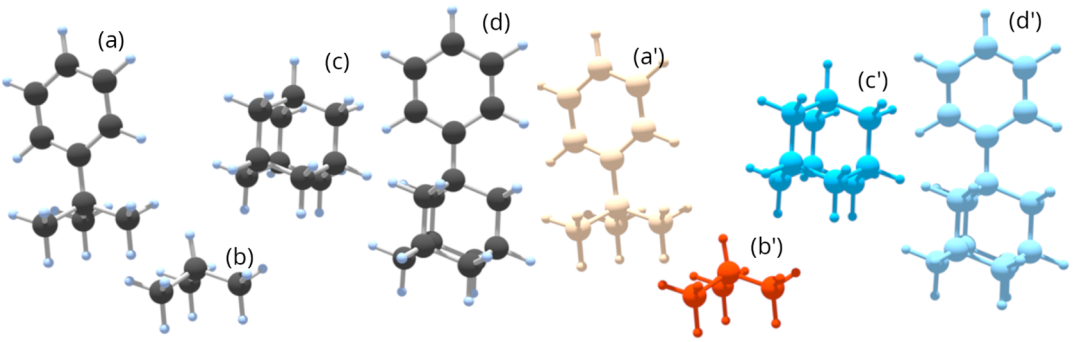

Figure 9. Investigated *substructures* of [AdPh] (d): [CMe_3Ph] (a), [CMe_3H] (b), and [AdH] (c). The coloring for (a−d) identifies the species H in light blue and C in dark gray/black. The coloring for (a′−d′) does not identify the atomic species but matches the coloring for Figure 10.

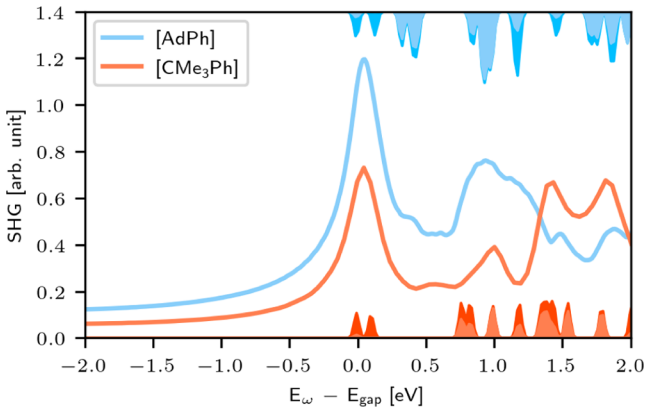

Figure 11. SHG response of [AdPh] in blue and [CMe_3Ph] in orange (solid lines) and DOS of both structures color coded correspondingly. The DOS in lighter colors is the partial density of states of the core atoms.

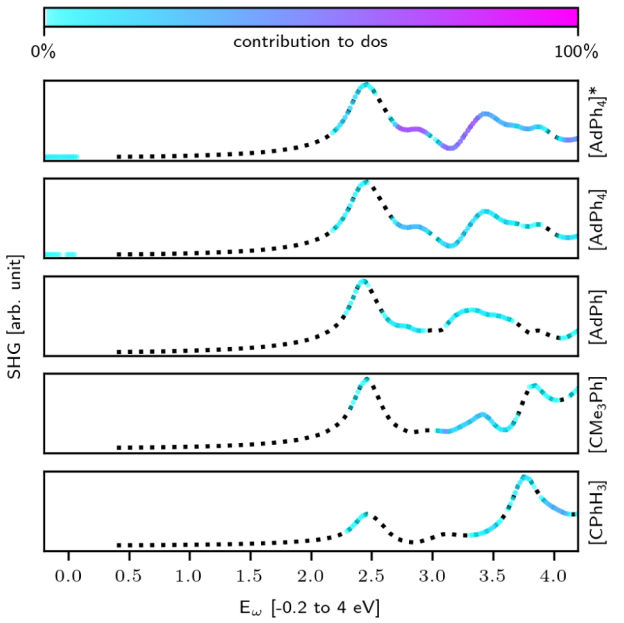

Figure 12. Total and partial DOS of [$AdPh_4$]*, [$AdPh_4$], [AdPh], [CMe_3Ph], and [$CPhH_3$] projected onto the SHG responses. The partial DOS refers to the core atom DOS. [$AdPh_4$]* labels a regular tetraphenyl adamantane cluster, [$AdPh_4$] the same structure for which the core atoms (all but the one directly connected with the phenyl substituents) are not considered for the calculation of the DOS. The SHG intensity of the single structures is arbitrarily scaled and not directly comparable.

colors. Both the DOS and the partial DOS of [AdPh] and [CMe_3Ph] are very similar, including the fact that the core contributions are visible in corresponding DOS peaks. Of course, the relative contribution of core states is higher for [AdPh], as it proportionally contains more core atoms. Figure 11 shows again that the first peak of the DOS of the substructures is due to the phenyl substituent and can thus represent only a target state from transitions from occupied levels in the substituent itself. As we shall see, this is a common feature of all investigated (tetra)phenyl adamantane derivatives.

Role of the Cluster Core. In the previous section, we have investigated the origin of the optical response of adamantane based molecular clusters and demonstrated that the clusters preserve the main characteristics of the SHG response of certain substructures. This also means that the characteristics of the SHG spectra in determined spectral regions are mostly defined by substructures and are not necessarily inherent only to the structure as a whole.

In this section, we investigate to which extent modifications of the core affect the SHG spectra, which are primarily defined by the substituents. In this context, we also investigate how a cluster with a specific core is affected by the number of substituents.

To explore this issue, we use tetraphenyl adamantane molecules as a model system, which we simplify step by step until a single [$CPhH_3$] cluster is reached. In particular, we follow the path [$AdPh_4$] → [AdPh] → [CMe_3Ph] → [$CPhH_3$]. [$AdPh_4$]* labels a regular tetraphenyl adamantane cluster, [$AdPh_4$] is the very same structure; however, the core C atoms are not considered for the calculation of the partial DOS (apart from the C atoms directly connected with the substituents).

Figure 12 shows the partial DOS of the considered structures projected onto the calculated SHG spectra. The latter are shifted on the energy axis so that the origin corresponds to the LUMO level. The core contribution to the DOS is color coded according to the color bar on the top. For the calculation of the [$AdPh_4$]* PDOS, the entire adamantane core is used, and the result is equivalent DOS and spectra shown, e.g., in Figure 4. For the calculation of [$AdPh_4$] PDOS, all core atoms excluding those directly connected to the substituents are discarded.

The projection of the DOS into the SHG spectrum shows that for all structures, as expected, the core atoms only contribute to the DOS at energies well beyond the first SHG peak. The comparison of [$AdPh_4$]* and [$AdPh_4$] also shows that limiting the DOS to the core connecting atoms does not substantially change the overall DOS, apart from the limited region at about 3 eV. This also means that only the core C atoms directly connected with the phenyl rings have some (very minor) contribution to the first DOS peak. Indeed, the core contribution of the systems in the last panels, where a single C atom—the one directly connected with the phenyl ring—builds the core, is very similar to the core contribution in [$AdPh_4$].

Further reducing the core size (bottom panels) only affects the side flank between 2.5 and 3 eV. Considering that from the top to the bottom panel of Figure 12, we are heavily modifying the considered cluster, removing 3 out of 4 Ph substituents and removing an entire adamantane core, the modifications of both SHG spectrum and DOS are surprisingly minor and occur in a very gradual way. The spectral signatures of a tetraphenyl adamantane cluster are already present in a [$CPhH_3$] substructure, although the spectral weights are, of course different. Following the principle of biomimetics, it might thus become possible to mimic the nonlinear optical response of large and complex molecules that are not computationally accessible by modeling the parts of the molecule that dominate the nonlinear optical response.

Finally, we present in this section the contribution to the DOS by the atoms not considered in Figure 12. This is displayed in Figure 13 with the same representation employed in Figure 12; however, the considered partial DOS is that of the substituent substructures and not that of the core atoms. In agreement with the calculations presented so far, the first SHG peak corresponds to a high DOS of the substituent atoms, irrespective of the number of phenyl rings or core atoms. At energies corresponding to the spectral regions about 3 eV, the substituent contribution is minor and increases again in correspondence of the spectral signatures located above 3.5 eV.

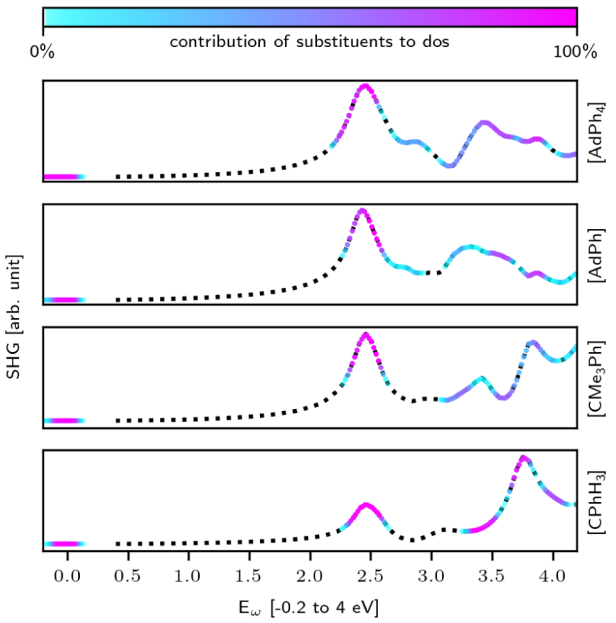

Figure 13. Partial DOS of the substituents [$AdPh_4$], [AdPh], [CMe_3Ph], and [$CPhH_3$] projected onto the SHG spectra, scaled to share the energy axis. The SHG intensity is scaled arbitrarily for each structure and is not directly comparable.

In the previous sections, we have discussed the optical response of organic molecular clusters, featuring either an adamantane core or a single carbon atom core and Ph substituents. We have concluded that it is possible to distinguish between core and substituent contributions to the SHG spectrum, at least to a qualitative degree. In this section, we investigate the effect of several different substituents and core compositions on the nonlinear optical response.

Figure 14 shows the SHG response of tetraphenyl tetrels with different central atoms within group 14. The calculated spectra

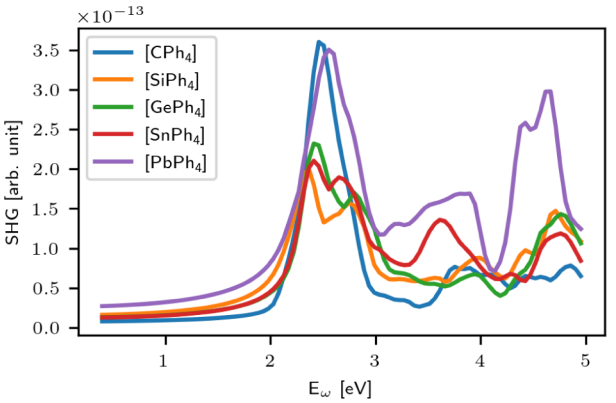

Figure 14. SHG response of tetraphenyl tetrels with C, Si, Ge, Sn, and Pb as central atom. The top and bottom group 14 elements C and Pb behave differently from Si, Ge, and Sn.

are in very good agreement with previous results[26] and show that the core atom can have a significant impact in the nonlinear optical response, although the latter has its origin in the phenyl substituents. We observe that the first spectral feature for all investigated tetraphenyl tetrels is the typical peak above 2 eV originating in the substituents and already tetraphenyl adamantane. This peak is followed by a second peak at a distance that depends on the central atom. For Si, Ge, and Sn, the peaks are separated. For Pb, the peaks are so close that they appear as a single peak of high intensity with a shoulder; for C, the second peak can be only intuited by the asymmetric form of the main peak.

This is also visible in Figure 15, which relates the SHG signal to the core contribution to the DOS. As for the tetraphenyl

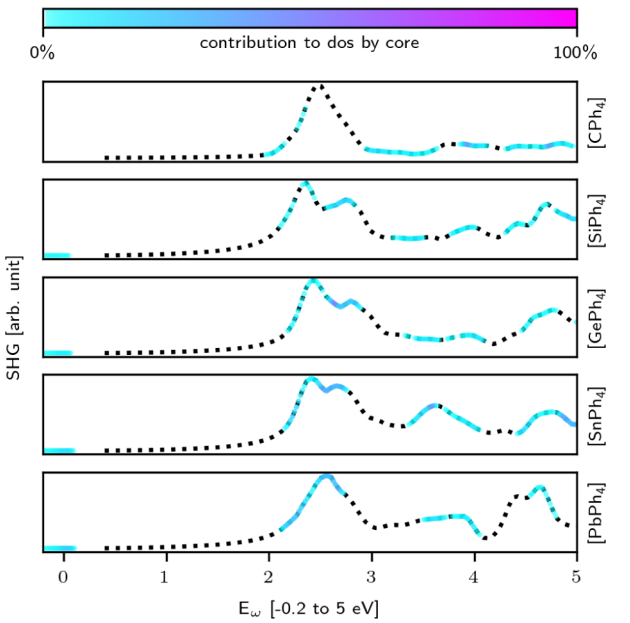

Figure 15. Partial DOS of the core atoms projected onto the SHG response of tetraphenyl tetrels, sharing the energy axis. The SHG intensity is scaled arbitrarily for each structure and is not directly comparable.

adamantane clusters, the core contribution is overall very low (light blue color of the DOS). Some contribution is visible at the second peak, which might explain the difference between the optical spectra of the clusters. For C, no contribution at all can be observed; for the other tetrels, a nonvanishing contribution with a tetrel specific extent is calculated.

Finally, we investigate how modifications of the adamantane core influence the optical response of the tetraphenyl adamantane cluster. The first modification we model is the substitution of all of the core atoms connected to the substituents with other elements of group 14 (Si, Ge, Sn). The corresponding results are shown in Figure 16.

The heterogeneous core composition strongly enhances the intensity of the SHG response with respect to the original adamantane cluster (blue line) and slightly modifies the spectrum so that it resembles that of the tetraphenyl tetrels shown in Figure 14. The Sn modified core is less effective in enhancing the SHG intensity with respect to the Si or Ge modifications. This can be attributed to electronic transitions spread over a larger energy range, thus resulting in a broader, lower SHG peak.

Furthermore, the analysis of the contribution to the DOS of the exchanged atoms (shown in Figure 17) shows a somewhat different behavior of the Sn substituted adamantane than that of the Si or Ge substituted cores. The contribution of the exchanged atoms grows with atomic numbers and shifts to lower energies, thus causing a redistribution of the spectral weights. We moreover observe that also the DOS analysis

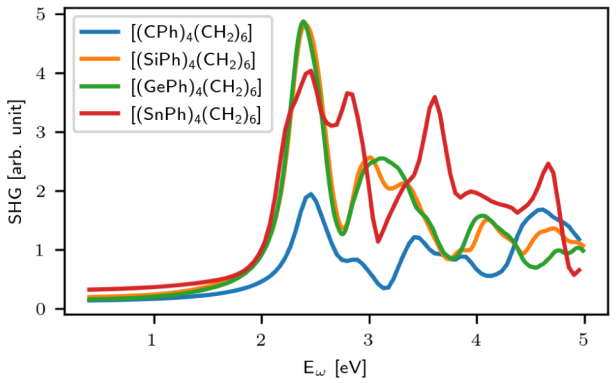

Figure 16. SHG response of a tetraphenyl adamantane cluster with a modified adamantane core. The modification consists in the substitution of all the C atoms connected to the phenyl substituents by a different group 14 element.

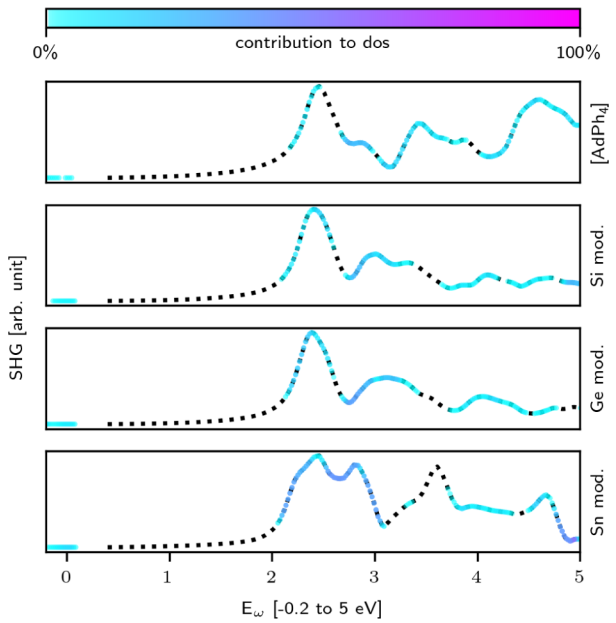

Figure 17. SHG response of modified tetraphenyl adamantane molecules. The clusters are modified so that the four C core atoms connected to the substituents are substituted by Si, Ge, and Sn, respectively. The SHG intensity is scaled arbitrarily for each structure and is not directly comparable. The contribution to the DOS of the core atoms connected with the phenyl substituents is projected as in the other figures onto the SHG response.

corroborates the similarities of the modified tetraphenyl adamantane clusters with the corresponding tetraphenyl tetrels (Figures 15 and 17).

Group 14 substituted adamantane cores are the subject of a dedicated investigation and will not be further discussed in this work.

Role of the Substituents. We now turn on the influence of the substituent field on the nonlinear optical properties of the molecular clusters. We showcase at first how different substituents affect the HOMO−LUMO gap and thus the optical response; then, we explore the role of the number of substituents and of a heterogeneous substituent field.

At the beginning of this section, we have demonstrated that the optical nonlinearity of the investigated tetraphenyl clusters has its origin in the phenyl rings. Yet, clusters composed of different substituents are characterized by strong optical nonlinearities as well.[25] Our calculations confirm the experimental findings. In order to disentangle the properties of the substituent field from those of the core as much as possible, we studied the effect of clusters composed of a single C atom and a homogeneous substituent field. Figure 18 shows the SHG

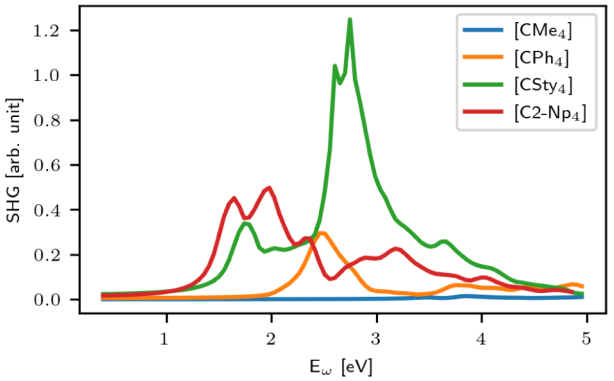

Figure 18. SHG response of molecular clusters consisting of a single carbon atom core and different homogeneous substituent fields.

spectra of such clusters with Me, Ph, Sty (styrene), and 2-Np (naphthyl) substituents. Very large differences concerning both the spectral features and intensities of the SHG peaks are predicted. Clusters with Me substituents (solid blue line) have vanishing second order optical response. 2-Np (solid red line) and to a much larger extent Sty (solid green line) are characterized by larger optical nonlinearities than the tetraphenyl clusters previously discussed (solid orange line). Interestingly, the onset of the nonlinear optical response for 2-Np and Sty clusters is located at much lower energies than for Ph clusters, which might prove very advantageous in WLE applications. Of course, the onset of the optical response depends on the HOMO−LUMO gap of the considered clusters. The relationships between the electronic gap and optical response are further investigated at the end of this section. We now turn to molecular clusters with nonhomogeneous substituent fields.

As an example, we discuss the substitution of a single Me substituent with a Ph ring. Figure 19 shows in the usual representation the nonlinear optical response of molecular clusters consisting of a group 14 atom core and an heterogeneous substituent field featuring one Ph ring and three Me groups. The SHG spectra of [CMe_3Ph], [$SiMe_3Ph$], [$GeMe_3Ph$], and [$SnMe_3Ph$] show only very minor deviations from the corresponding spectra calculated for a homogeneous phenyl substituent field as shown in Figure 15. This means, on the one hand, that the phenyl substituent is a substructure with dominating character in the low energy region of the nonlinear optical response. On the other hand, it means that the heterogeneous substituent field does not drastically influence the SHG spectrum.

In further similarity with Figure 15, we observe that the contribution of the central atom to the DOS is limited, with a nonvanishing share only in correspondence of the second peak for the heavier tetrels.

Another aspect that we investigate is the impact of the number of substituents on the optical properties of the molecular clusters. The number of substituents affects the second order optical response of the tetraphenyl tetrels in a nonlinear manner.

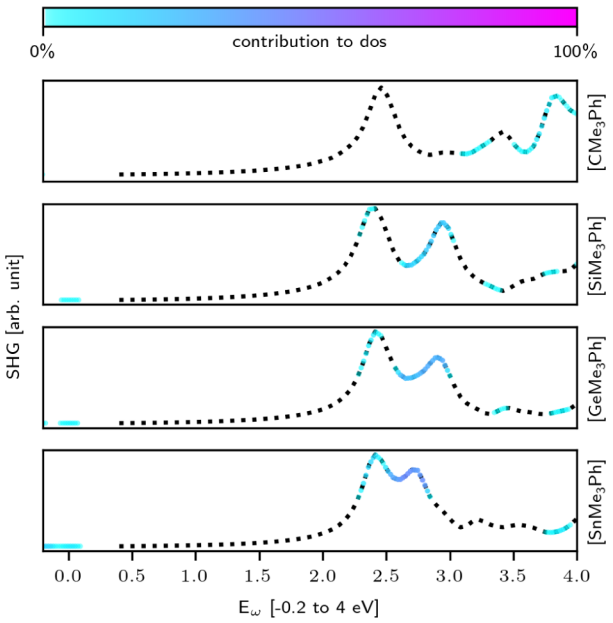

Figure 19. SHG response of XMe_3Ph clusters with X = C, Si, Ge, and Sn and core contribution to the density of states. The SHG intensity is scaled arbitrarily for each structure and is not directly comparable.

This can be observed in Figure 20, where we show the optical response obtained adding the substituents stepwise. In the figure, two energy ranges between 2 and 4 eV are highlighted, where the evolution of the signal with the number of substituents is best observed. The spectra calculated with 1 and 2 substituents are rather similar, exactly as the spectra calculated for 3 and 4 substituents. However, the first SHG peak exhibits a rather sudden jump between the two and three substituents. This is not the case for carbon and lead tetraphenyl, where increasing or decreasing the number of substituents has a gradual effect on the nonlinear optical response. Again, C and Pb behave differently from the rest of group 14. Whether this can be explained by the peculiarity of the C−C bond (in the case of C) or, e.g., by relativistic effects (in the case of Pb), remains to be ascertained in the following investigations.

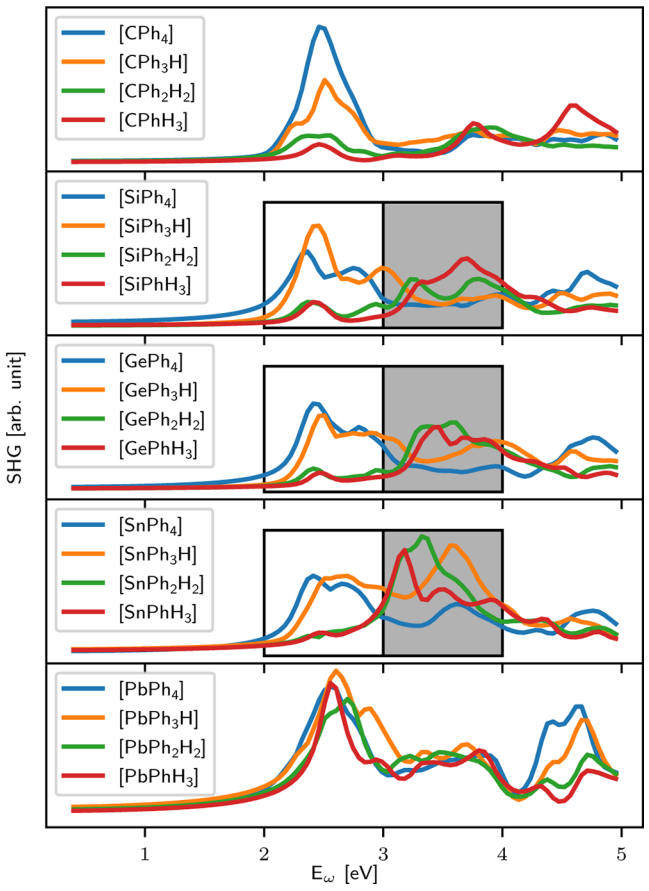

Figure 20. SHG response of C, Si, Ge, Sn, and Pb phenyl tetrels for an increasing number of substituents. Two energy ranges are highlighted in which the evolution of the spectra is clearly observable.

The large differences in the SHG response predicted for clusters with different substituents suggest that by carefully blending the substituents, a manipulation of the optical nonlinearities might become possible. In particular, tuning the energy of the HOMO−LUMO transition may provide control over the onset of the optical response.

The DFT calculated HOMO−LUMO gaps of homogeneous $[Me_4C]$, $[Ph_4C]$, $[Sty_4C]$, and $[2\text{-}Np_4C]$ clusters are shown in Figure 21. According to the color coding of Figure 18, Me is in blue, Ph in orange, Sty in green, and 2-Np in red. The electronic gaps calculated for intermediate cluster obtained substituting stepwise the substituents $[2\text{-}Np_4C] \rightarrow [Sty_4C] \rightarrow [Ph_4C] \rightarrow [Me_4C]$ are color coded in colors of a gradient from one structure to another.

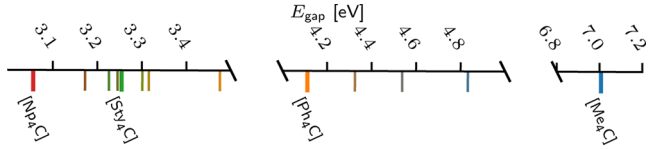

Figure 21. DFT calculated HOMO−LUMO energy gaps of $[Me_4C]$ (blue), $[Ph_4C]$ (orange), $[Sty_4C]$ (green), and $[2\text{-}Np_4C]$ (red). The HOMO−LUMO gaps of the hybrid structures obtained by stepwise substituent substitution $[Me_4C] \rightarrow [Ph_4C] \rightarrow [Sty_4C] \rightarrow [2\text{-}Np_4C]$ are colored in a gradient corresponding to the number of substituted substituents.

The calculated HOMO−LUMO gap varies generally gradually between two homogeneous clusters, although deviations are present. As well, the first substitution has in each case the largest effect on the electronic gap.

To further investigate this aspect, we calculated the transitional SHG responses of heterogeneous clusters. Figure 22 shows the SHG response for the selected structures $[Me_4C]$, $[Me_3PhC]$, $[Ph_4C]$, $[Ph_3StyC]$, $[Sty_4C]$, $[Sty_32\text{-}NpC]$, and $[2\text{-}Np_4C]$. The SHG response of the heterogeneous clusters included in each of the three graphs exhibits a sudden shift toward one of the two homogeneous structures. After the first shift, the response gradually approaches the SHG spectrum of the target homogeneous cluster. This corresponds to the gradual change in the HOMO−LUMO gap as shown in Figure 21.

Tuning the Optical Response. In Figure 20, it is shown that the intensity of the second order optical response of a given molecular cluster can be modified by the number of substituents, at least for molecular clusters with a single-atom (group 14) core. We show in Figure 23, where the SHG spectra for clusters with adamantane core and a different number of substituents are plotted, that this is also true for more complex cores.

The SHG spectrum of the adamantane core (black solid line) is modified by the presence of the phenyl rings by an amount

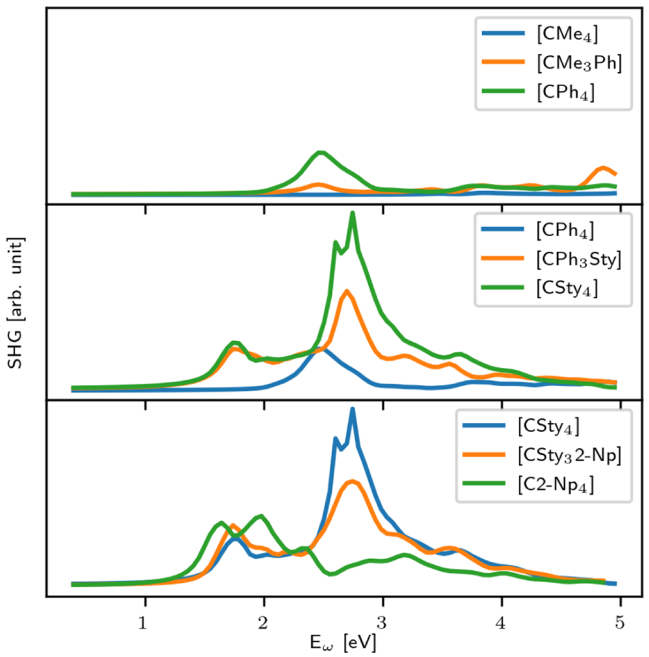

Figure 22. SHG response of the cluster structures [Me_4C],[Me_3PhC], [Ph_4C], [Ph_3StyC], [Sty_4C], [$Sty_3$2-NpC], and [2-Np_4C].

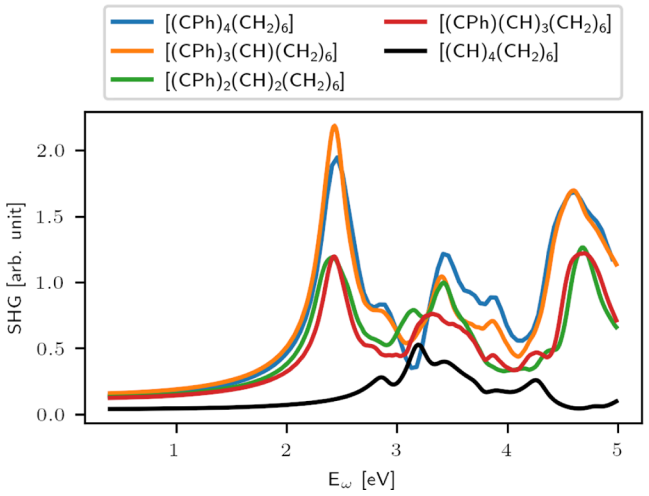

Figure 23. SHG response of an adamantane cluster with *n*-phenyl substituents, $n \in 0, \ldots, 4$.

depending on the number of substituents. The characteristic peak just above 2 eV and related to the substituents grows nonlinearly with the number of phenyl rings and has a jump in intensities between clusters with 4 or 3 rings and clusters with 2 or 1 rings. A similar behavior was encountered for the clusters with single atom core structures and shown in Figure 20 (with the exception of the cluster with carbon as a central atom).

Yet, modifying the number of substituents of the single cluster is not the only way to modify the intensity of the optical response. A further possible approach exploits the *ensemble* properties of the substances instead of modifications of the single clusters.

Recent investigations have shown that the molecular clusters investigated in this work can be (at least partially) synthesized with a different habitus.[49] In particular, mixtures can be produced in which the clusters form dimers with a different degree of symmetry. As the structure symmetry is crucial for the optical response (e.g., only noncentrosymmetric clusters can have a nonvanishing SHG intensity), the formation of dimers opens different possibilities to tune the optical response without modifying the chemical composition of the constituents.

In the following, we demonstrate this possibility by showing the gradual modification of the SHG intensity of different dimer structures and correlating it with the degree of symmetry. In particular, we quantify the deviation from centrosymmetry by the tolerance threshold (Å) necessary to identify the structures as centrosymmetric.

As a general rule of thumb, the overall symmetry of a cluster can be enhanced or reduced by the modification of the core structure, the habitus, and as well by modifying the substituent type or their combination.[18]

Figure 24A shows a low symmetry [(2-NpSi)-$(CH_2)_4(PhSn)_3S_3$] cluster, Figure 24B a dimer structure

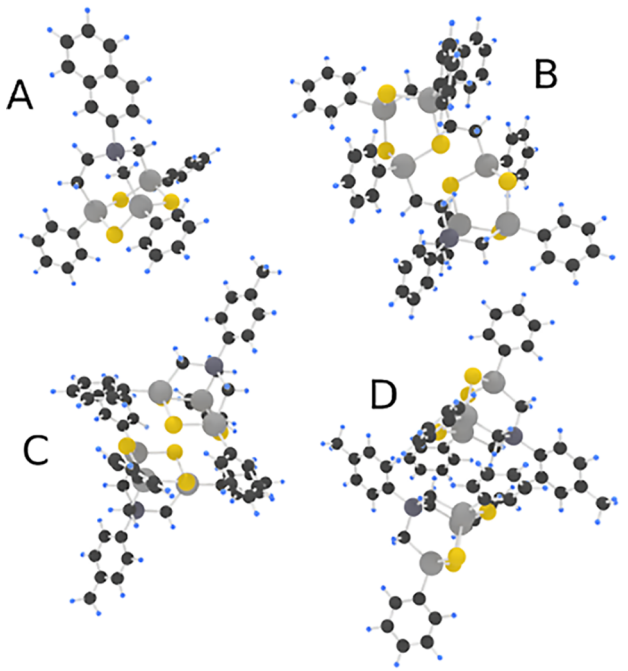

Figure 24. (A) Isolated [(2-NpSi)$(CH_2)_4(PhSn)_3S_3$] cluster, (B) [(PhSi)$(CH_2)_4(PhSn)_3S_3]_2$ dimer, in the text referred to as fused core dimer, and (C,D) [(TolSi)$(CH_2)_3(PhSn)_3S_3]_2$ dimers in different configurations. Sn atoms are colored light gray, Si dark gray, and S yellow. C and H atoms are colored in black and light blue, respectively.

referred to as a *fused* core, and Figure 24C,D are dimer structures which are predicted for the [(TolSi)-$(CH_2)_3(PhSn)_3S_3]_2$ cluster in the gas phase and in a crystal structure, respectively (with Tol referring to tolyl). The corresponding SHG spectra are listed in Figure 25. Please notice the logarithmic scale spanning several orders of magnitude. The spectra with vanishing intensities are affected by larger relative numerical errors; however, they still give the correct magnitude of the SHG intensity.

The SHG of structure A is of similar magnitude as the SHG spectra calculated for tetraphenyl molecules with composite cores. The formation of dimers with fused cores B brings the whole structure toward a nearly centrosymmetric configuration, and although the deviation from inversion symmetry is still substantial, the SHG intensity is quenched by 2 orders of magnitude. Dimer structures C and D even closer to inversion symmetry are characterized by even smaller SHG intensities; in

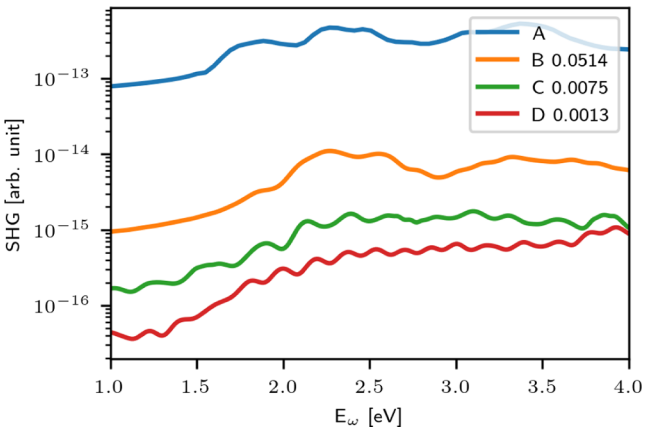

Figure 25. SHG response of structures with a different deviation from the inversion symmetry. (A) $[(2\text{-NpSi})(CH_2)_4(PhSn)_3S_3]$, (B) $[(PhSi)(CH_2)_4(PhSn)_3S_3]_2$, (C,D) $[(TolSi)(CH_2)_3(PhSn)_3S_3]_2$. (C,D) only by the orientation of their substructures.

particular, the dimer extracted from the molecular crystal has a nonvanishing but extremely low SHG response, correlating with the small deviation from centrosymmetry.

Before concluding, we provide a general remark about the molecular clusters with high optical nonlinearities. We started the investigation with tetraphenyl tetrels or tetraphenyl adamantanes. They can be synthesized to feature different numbers of phenyl rings. They can also be modified by substituting one or more substituents, e.g., by Me, 2-Np, or Sty, which exponentially enhances the number of possible configurations. Modifications of the adamantane core by substitution of C with group 14 elements, as well as the synthesis of further nonorganic cores (e.g., those including chalcogens[18]) substantially widen the phase space of possible compounds to many thousands of clusters.[50] Different habitus, laser-induced distortions[51] further provide modifications of the optical response that can be possibly exploited to tune the optical properties of the compounds, either toward optimized WLG or toward further nonlinear effects such as SHG. An exhaustive, thorough investigation of all the mentioned modifications is, however, actually beyond reach and outside the goal of the present work.

CONCLUSIONS

The nonlinear optical response of (hetero)adamantane-based molecular clusters with general formula $[(RT)_4E_6]$ and $[R_4T]$ (T = group 14, R = organic substituents, E = S, CH_2) has been investigated within DFT. We have shown how changes in the composition of otherwise geometrically similar structures can tune, e.g., the SHG response. Importantly, we find that certain spectral features are associated with specific cluster substructures. These spectral signatures are inherited in the optical response of the clusters if they are modified to include the corresponding substructure. Moreover, we find some substructures to be dominant in their effects on the SHG response. If a specific substructure is not dominant, we can assume a gradual change in the SHG response fitting to the gradual change of the structure, in contrast to the introduction of a dominant substituent which causes an *instantaneous* shift in the optical response. Additionally, we observe that the number of substituents can change the SHG response to a large extent. While the position of the spectral signatures on the energy axis does not change significantly, the intensity up to 3 eV (or more generally, of the first major peak) can increase sharply when going from 2 to 4 substituent structures. The substituent structures could be identified as the major contributor to the SHG response, especially for the first peak. Furthermore, the substituent structure primarily defines the more general characteristic up to around 3 eV. This result can be understood by considering the electronic transitions between the electronic energy eigenvalues and the spatial localization of the corresponding orbitals. The results show that these orbitals are most dominantly located on the substituent substructures.

Considering the variety of possible substituents and changes that can be introduced to an adamantane like core substructure, the investigated structures as well as further modifications offer great potential for a tuned optical response.

We also showed how the adamantane cores influence the nonlinear optical response above ca. 3 eV. Further investigations of molecular clusters with cores of different symmetry and composition shall reveal whether different cluster cores can affect the optical nonlinearities in different energy ranges. Investigations of different core structures such as cubane or diamantane could offer more insight into the impact of core symmetry and relative substituent orientation on the optical response.

ASSOCIATED CONTENT

Data Availability Statement

Atom coordinates are provided in the Supporting Information. An overview of how computational parameters were chosen for nonlinear optical calculations is provided in the Supporting Information. Further computational details will be provided upon reasonable request. To do so, please contact Ferdinand Ziese.

AUTHOR INFORMATION

Corresponding Authors

Ferdinand Ziese − *Institut für Theoretische Physik and Center for Materials Research (LaMa/ZfM), Justus-Liebig-Universität Gießen, Gießen 35392, Germany;* orcid.org/0009-0003-6855-9708; Email: ferdinand.ziese@physik.uni-giessen.de

Jie Wang − *Karlsruhe Institute of Technology (KIT), Institute of Nanotechnology, Karlsruhe 76131, Germany;* Email: jie.wang@kit.edu

Irán Rojas León − *Karlsruhe Institute of Technology (KIT), Institute of Nanotechnology, Karlsruhe 76131, Germany;* Email: iran.leon@kit.edu

Stefanie Dehnen − *Karlsruhe Institute of Technology (KIT), Institute of Nanotechnology, Karlsruhe 76131, Germany;* orcid.org/0000-0002-1325-9228; Email: stefanie.dehnen@kit.edu

Simone Sanna − *Institut für Theoretische Physik and Center for Materials Research (LaMa/ZfM), Justus-Liebig-Universität Gießen, Gießen 35392, Germany;* orcid.org/0000-0003-4416-0252; Email: simone.sanna@theo.physik.uni-giessen.de

Author Contributions

F.Z. and S.S. conceived the project. F.Z. performed the calculations and analysis with support from S.S., S.D, J.W, and I.R.L. The manuscript was written by F.Z. and S.S. and contributed by all authors. All authors reviewed the manuscript.

Notes

The authors declare no competing financial interest.

ACKNOWLEDGMENTS

This work is supported by the German Research Foundation (DFG) through the research group FOR2824 (Grant No. 398143140). Calculations for this research were conducted on the Lichtenberg high performance computer of the TU Darmstadt and at the Höchstleistungsrechenzentrum Stuttgart (HLRS). The authors furthermore acknowledge the computational resources provided by the HPC Core Facility and the HRZ of the Justus-Liebig-Universität Gießen.

ADDITIONAL NOTES

[1]S. Dehnen, private communication.

[2]This can differ from the displayed lines where we force this delta to be at least $\min(\Delta E)_{\mathrm{vis}} = 0.01$ eV. We also force a $\min(\Delta E)_{*} = 0.01$ eV, which is used to calculate a convolution (of step functions with the width ΔE) between the origin orbital groups o (being the occupied orbitals) and a specific target orbital group t (being the unoccupied orbitals)."

[3]This is skewed for $\min(\Delta E)_{*} = 0.01$ eV.

[4]The densities ρ_o and ρ_t in Figure 5 are not normalized by the number of states in the respective orbital group as done in Figure 3. The presented isosurface is the result of choosing the middle value of the data range and multiplying that value by $\frac{1}{4}$. The value is arbitrarily chosen to provide a clearly represented isosurface.

REFERENCES

(1) Panday, S. R.; Fregoso, B. M. Strong second harmonic generation in two-dimensional ferroelectric IV-monochalcogenides. *J. Phys.: Condens. Matter* **2017**, *29*, 43LT01.

(2) Cheng, M.; Zhu, Z.-Z.; Guo, G.-Y. Strong bulk photovoltaic effect and second-harmonic generation in two-dimensional selenium and tellurium. *Phys. Rev. B* **2021**, *103*, 245415.

(3) Kang, L.; Lin, Z. Second harmonic generation of $MoSi_2N_4$-type layers. *Phys. Rev. B* **2021**, *103*, 195404.

(4) Marino, G.; Gigli, C.; Rocco, D.; Lemaître, A.; Favero, I.; De Angelis, C.; Leo, G. Zero-Order Second Harmonic Generation from AlGaAs-on-Insulator Metasurfaces. *ACS Photonics* **2019**, *6*, 1226−1231.

(5) Gao, Y.; Shadrivov, I. V. Second harmonic generation in graphene-coated nanowires. *Opt. Lett.* **2016**, *41*, 3623−3626.

(6) Klee, B. D.; Dornsiepen, E.; Stellhorn, J. R.; Paulus, B.; Hosokawa, S.; Dehnen, S.; Pilgrim, W.-C. Structure Determination of a New Molecular White-Light Source. *Phys. Status Solidi b* **2018**, *255*, 1800083.

(7) Rosemann, N. W.; Locke, H.; Schreiner, P. R.; Chatterjee, S. White-Light Generation through Nonlinear Optical Response of 1,3,5,7-Tetraphenyladamantane: Amorphous versus Crystalline States. *Adv. Opt. Mater.* **2018**, *6*, 1701162.

(8) Li, D.; Hu, W.; Wang, J.; Zhang, Q.; Cao, X.-M.; Ma, X.; Tian, H. White-light emission from a single organic compound with unique self-folded conformation and multistimuli responsiveness. *Chem. Sci.* **2018**, *9*, 5709−5715.

(9) Alfano, R. R. The Ultimate White Light. *Sci. Am.* **2006**, *295*, 86−93.

(10) Akimov, D.; Schmitt, M.; Maksimenka, R.; Dukel'skii, K.; Kondrat'ev, Y. N.; Khokhlov, A.; Shevandin, V.; Kiefer, W.; Zheltikov, A. Supercontinuum generation in a multiple-submicron-core microstructure fiber: Toward limiting waveguide enhancement of nonlinear-optical processes. *Appl. Phys. B: Laser Opt.* **2003**, *77*, 299−305.

(11) Guignard, M.; Nazabal, V.; Troles, J.; Smektala, F.; Zeghlache, H.; Quiquempois, Y.; Kudlinski, A.; Martinelli, G. Second-harmonic generation of thermally poled chalcogenide glass. *Opt. Express* **2005**, *13*, 789−795.

(12) Nakamura, S.; Mukai, T.; Senoh, M. High-brightness InGaN/AlGaN double-heterostructure blue-green-light-emitting diodes. *J. Appl. Phys.* **1994**, *76*, 8189−8191.

(13) Nakamura, S. Nobel Lecture: Background story of the invention of efficient blue InGaN light emitting diodes. *Rev. Mod. Phys.* **2015**, *87*, 1139−1151.

(14) Poriel, C.; Rault-Berthelot, J. Blue Single-Layer Organic Light-Emitting Diodes Using Fluorescent Materials: A Molecular Design View Point. *Adv. Funct. Mater.* **2020**, *30*, 1910040.

(15) Gotta, J.; Shalom, T. B.; Aslanoglou, S.; Cifuentes-Rius, A.; Voelcker, N. H.; Elnathan, R.; Shoseyov, O.; Richter, S. Stable White Light-Emitting Biocomposite Films. *Adv. Funct. Mater.* **2018**, *28*, 1706967.

(16) Su, H.-C.; Chen, Y.-R.; Wong, K.-T. Recent Progress in White Light-Emitting Electrochemical Cells. *Adv. Funct. Mater.* **2020**, *30*, 1906898.

(17) Wu, J.; Zheng, G.; Liu, X.; Qiu, J. Near-infrared laser driven white light continuum generation: Materials, photophysical behaviours and applications. *Chem. Soc. Rev.* **2020**, *49*, 3461−3483.

(18) Rojas-León, I.; Christmann, J.; Schwan, S.; Ziese, F.; Sanna, S.; Mollenhauer, D.; Rosemann, N. W.; Dehnen, S. Cluster-Glass for Low-Cost White-Light Emission. *Adv. Mater.* **2022**, *34*, 2203351.

(19) Beetar, J. E.; Nrisimhamurty, M.; Truong, T.-C.; Nagar, G. C.; Liu, Y.; Nesper, J.; Suarez, O.; Rivas, F.; Wu, Y.; Shim, B.; et al. Multioctave supercontinuum generation and frequency conversion based on rotational nonlinearity. *Sci. Adv.* **2020**, *6*, No. eabb5375.

(20) Meng, F.; Lapre, C.; Billet, C.; Sylvestre, T.; Merolla, J.-M.; Finot, C.; Turitsyn, S. K.; Genty, G.; Dudley, J. M. Intracavity incoherent supercontinuum dynamics and rogue waves in a broadband dissipative soliton laser. *Nat. Commun.* **2021**, *12*, 5567.

(21) Fan, R.; Lin, Y.-Y.; Chang, L.; Boes, A.; Bowers, J.; Liu, J.-W.; Lin, C.-H.; Wang, T.-K.; Qiao, J.; Kuo, H.-C.; et al. Higher order mode supercontinuum generation in tantalum pentoxide (Ta2O5) channel waveguide. *Sci. Rep.* **2021**, *11*, 7978.

(22) Xiang, H.; Wang, R.; Chen, J.; Li, F.; Zeng, H. Research progress of full electroluminescent white light-emitting diodes based on a single emissive layer. *Light: Sci. Appl.* **2021**, *10*, 206.

(23) Rosemann, N. W.; Eußner, J. P.; Beyer, A.; Koch, S. W.; Volz, K.; Dehnen, S.; Chatterjee, S. A highly efficient directional molecular white-light emitter driven by a continuous-wave laser diode. *Science* **2016**, *352*, 1301−1304.

(24) Rosemann, N. W.; Eußner, J. P.; Dornsiepen, E.; Chatterjee, S.; Dehnen, S. Organotetrel Chalcogenide Clusters: Between Strong Second-Harmonic and White-Light Continuum Generation. *J. Am. Chem. Soc.* **2016**, *138*, 16224−16227.

(25) Dehnen, S.; Schreiner, P. R.; Chatterjee, S.; Volz, K.; Rosemann, N. W.; Pilgrim, W.-C.; Mollenhauer, D.; Sanna, S. Amorphous Molecular Materials for Directed Supercontinuum Generation. *ChemPhotochem* **2021**, *5*, 1033−1041.

(26) Eberheim, K.; Dues, C.; Attaccalite, C.; Müller, M. J.; Schwan, S.; Mollenhauer, D.; Chatterjee, S.; Sanna, S. Tetraphenyl Tetrel Molecules and Molecular Crystals: From Structural Properties to Nonlinear Optics. *J. Phys. Chem. C* **2022**, *126*, 3713−3726.

(27) Schmidt, F.; Riefer, A.; Schmidt, W. G.; Schindlmayr, A.; Imlau, M.; Dobener, F.; Mengel, N.; Chatterjee, S.; Sanna, S. Quasiparticle and excitonic effects in the optical response of KNbO3. *Phys. Rev. Mater.* **2019**, *3*, 054401.

(28) Dues, C.; Müller, M. J.; Chatterjee, S.; Attaccalite, C.; Sanna, S. Nonlinear optical response of ferroelectric oxides: First-principles calculations within the time and frequency domains. *Phys. Rev. Mater.* **2022**, *6*, 065202.
(29) Müller, M. J.; Ziese, F.; Belz, J.; Hüppe, F.; Gowrisankar, S.; Bernhardt, B.; Schwan, S.; Mollenhauer, D.; Schreiner, P. R.; Volz, K.; et al. Octave-spanning emission across the visible spectrum from single crystalline 1,3,5,7-tetrakis-(p-methoxyphenyl)adamantane. *Opt. Mater. Express* **2022**, *12*, 3517−3529.
(30) Hanau, K.; Schwan, S.; Schäfer, M. R.; Müller, M. J.; Dues, C.; Rinn, N.; Sanna, S.; Chatterjee, S.; Mollenhauer, D.; Dehnen, S. Towards Understanding the Reactivity and Optical Properties of Organosilicon Sulfide Clusters. *Angew. Chem., Int. Ed.* **2021**, *60*, 1176−1186.
(31) Dornsiepen, E.; Dobener, F.; Mengel, N.; Lenchuk, O.; Dues, C.; Sanna, S.; Mollenhauer, D.; Chatterjee, S.; Dehnen, S. White-Light Generation Upon In-Situ Amorphization of Single Crystals of $[(Me_3P)_3AuSn(PhSn)_3S_6]$ and $[(Et_3P)_3AgSn(PhSn)_3S_6]$. *Adv. Opt. Mater.* **2019**, *7*, 1801793.
(32) Kresse, G.; Hafner, J. Ab initio molecular dynamics for liquid metals. *Phys. Rev. B* **1993**, *47*, 558−561.
(33) Kresse, G.; Furthmüller, J. Efficiency of ab-initio total energy calculations for metals and semiconductors using a plane-wave basis set. *Comput. Mater. Sci.* **1996**, *6*, 15−50.
(34) Kresse, G.; Furthmüller, J. Efficient iterative schemes for ab initio total-energy calculations using a plane-wave basis set. *Phys. Rev. B* **1996**, *54*, 11169−11186.
(35) Perdew, J. P.; Burke, K.; Ernzerhof, M. Generalized Gradient Approximation Made Simple. *Phys. Rev. Lett.* **1996**, *77*, 3865−3868.
(36) Blöchl, P. E. Projector augmented-wave method. *Phys. Rev. B* **1994**, *50*, 17953−17979.
(37) Kresse, G.; Joubert, D. From ultrasoft pseudopotentials to the projector augmented-wave method. *Phys. Rev. B* **1999**, *59*, 1758−1775.
(38) Grimme, S.; Antony, J.; Ehrlich, S.; Krieg, H. A consistent and accurate ab initio parametrization of density functional dispersion correction (DFT-D) for the 94 elements H-Pu. *J. Chem. Phys.* **2010**, *132*, 154104.
(39) Grimme, S.; Ehrlich, S.; Goerigk, L. Effect of the damping function in dispersion corrected density functional theory. *J. Comput. Chem.* **2011**, *32*, 1456−1465.
(40) Giannozzi, P.; Andreussi, O.; Brumme, T.; Bunau, O.; Nardelli, M. B.; Calandra, M.; Car, R.; Cavazzoni, C.; Ceresoli, D.; Cococcioni, M.; et al. Advanced capabilities for materials modelling with QUANTUM ESPRESSO. *J. Phys.: Condens. Matter* **2017**, *29*, 465901.
(41) Giannozzi, P.; Baroni, S.; Bonini, N.; Calandra, M.; Car, R.; Cavazzoni, C.; Ceresoli, D.; Chiarotti, G. L.; Cococcioni, M.; Dabo, I.; et al. QUANTUM ESPRESSO: A modular and open-source software project for quantum simulations of materials. *J. Phys.: Condens. Matter* **2009**, *21*, 395502.
(42) http://www.quantum-simulation.org/potentials/sg15_oncv/index.htm.
(43) Hamann, D. R. Optimized norm-conserving Vanderbilt pseudopotentials. *Phys. Rev. B* **2013**, *88*, 085117.
(44) Schlipf, M.; Gygi, F. Optimization algorithm for the generation of ONCV pseudopotentials. *Comput. Phys. Commun.* **2015**, *196*, 36−44.
(45) Attaccalite, C.; Grüning, M. Nonlinear optics from an ab initio approach by means of the dynamical Berry phase: Application to second- and third-harmonic generation in semiconductors. *Phys. Rev. B* **2013**, *88*, 235113.
(46) Souza, I.; Íñiguez, J.; Vanderbilt, D. Dynamics of Berry-phase polarization in time-dependent electric fields. *Phys. Rev. B* **2004**, *69*, 085106.
(47) Sangalli, D.; Ferretti, A.; Miranda, H.; Attaccalite, C.; Marri, I.; Cannuccia, E.; Melo, P.; Marsili, M.; Paleari, F.; Marrazzo, A.; et al. Many-body perturbation theory calculations using the yambo code. *J. Phys.: Condens. Matter* **2019**, *31*, 325902.
(48) Cole, J. M. Organic materials for second-harmonic generation: Advances in relating structure to function. *Philos. Trans. R. Soc., A* **2003**, *361*, 2751−2770.
(49) Schwan, S.; Achazi, A. J.; Ziese, F.; Schreiner, P. R.; Volz, K.; Dehnen, S.; Sanna, S.; Mollenhauer, D. Insights into molecular cluster materials with adamantane-like core structures by considering dimer interactions. *J. Comput. Chem.* **2023**, *44*, 843−856.
(50) Rinn, N.; Rojas-León, I.; Peerless, B.; Gowrisankar, S.; Ziese, F.; Rosemann, N. W.; Pilgrim, W.-C.; Sanna, S.; Schreiner, P. R.; Dehnen, S. Adamantane-type clusters: Compounds with a ubiquitous architecture but a wide variety of compositions and unexpected materials properties. *Chem. Sci.* **2024**, *15*, 9438−9509.
(51) Belz, J.; Haust, J.; Müller, M. J.; Eberheim, K.; Schwan, S.; Gowrisankar, S.; Hüppe, F.; Beyer, A.; Schreiner, P. R.; Mollenhauer, D.; et al. Adamantanes as White-Light Emitters: Controlling the Arrangement and Functionality by External Coulomb Forces. *J. Phys. Chem. C* **2022**, *126*, 9843−9854.